Binding of Agonist WAY-267,464 and Antagonist WAY-Methylated to Oxytocin Receptor

Probed by All-Atom Molecular Dynamics Simulations

Abdullahi Ibrahim Uba^{1§}, Christina Radicella^{2§}, Carolyn Readmond², Nicolas Scorese², Siyan

Liao^{2,3}, Haiguang Liu^{1*} and Chun Wu^{2*}

¹ Complex Systems Division, Beijing Computational Science Research Center, Beijing 100193,

China

² College of Science and Mathematics, Rowan University, Glassboro, NJ, 08028 USA

³ Key Laboratory of Molecular Target & Clinical Pharmacology, School of Pharmaceutical

Sciences, Guangzhou Medical University, Guangzhou, 511436, China

§: Both authors contributed equally to this work

* To whom correspondence should be addressed: Chun Wu: wuc@rowan.edu;

Haiguang Liu: hgliu@csrc.ac.cn

1

Abstract

Aims: Non-peptide ligands of oxytocin receptor (OTR) have promising potentialities as therapeutic agents with improved pharmacological properties. WAY-267,464 is a non-peptide agonist which loses its agonist activity when its resorcinol moiety is methylated, yielding a partial antagonist (denoted here, WAY-Methylated). This study attempts to rationalize these opposing activities by comparative analyses of structural dynamics of OTR in complex with these ligands.

Main methods: Glide extra precision (XP) docking with and without positional constraints was employed to probe alternative binding poses of both WAY-267,464 and WAY-Methylated. The more preferred configuration of each system was subjected to an extended 2 μs MD simulation and the physics-based Molecular Mechanics-Generalized Born Surface Area (MM-GBSA) binding energy was used to rank the complexes with improved accuracy, in addition to empirical-based Glide docking score. Network analysis was performed, and the identified critical residues were cross-referenced with the experimental mutagenesis data.

Key findings: The added methyl groups in the antagonist WAY-Methylated enhanced hydrophobicity, resulting in a flipped binding pose deeper in the binding pocket. Interestingly, OTR responded to the methylation by stabilizing the initial inactive conformation, decreasing fluctuations and increasing the overall secondary structural composition. Conversely, the agonist WAY-267,464 produced larger fluctuations to allow the receptor to change from the default inactive state to a state of partial activation. These transitions were further supported by the identified critical residues overlapping with experimental mutagenesis data.

Significance: These findings provide insights into the activation mechanism of OTR by WAY-267.464 and its antagonism by WAY-Methylated.

Keywords: Oxytocin receptor, WAY-267,464, WAY-Methylated, Molecular docking, MD simulation, MM-GBSA

Abbreviations: OTR, Oxytocin receptor; MD, molecular dynamics; MM-GBSA, molecular mechanics generalized Born surface area; GPCR, G-protein-coupled receptor; TM, transmembrane; ICL, intracellular loop; ECL, extracellular loop; POPC, 1-palmitoyl-2-oleoyl-sn-phosphatidylcholine; SID, simulation interaction diagram; RMSD, root mean square deviation; RMSF, root mean square fluctuation; XP, extra precision;

Introduction

The oxytocin receptor (OTR) is closely related to the three classes of vasopressin receptors, V_{1A}, V_{1B}, and V₂, which all belong to the family A (rhodopsin-like) G-protein coupled receptors (GPCR) [1-20]. Previous studies have shown that many key residues important for ligand binding are conserved between these receptors, which makes the finding of a selective ligand for either of the receptors very challenging. Endogenous oxytocin acts as an agonist and is used in combination with synthetic oxytocin to intravenously induce labor [6, 18, 20-24]. OTR peptide antagonists are currently used to delay labor—specifically preventing preterm labor. However, these peptide antagonists are typically not selective for the OTR only, resulting in many undesirable side effects: they cannot be administered orally as they get degraded too quickly within the gastrointestinal tract, and are hard to get past the blood-brain barrier [1, 12, 13, 17, 20, 25-27]. Non-peptide ligands have promising potential to become orally bioavailable drugs with improved selectivity, and longer lasting effects. They could be used to possibly treat other medical conditions such as erectile dysfunction and anxiety disorders [1, 12, 17, 20, 25-29]. Currently, there are no FDA-approved non-peptide OTR ligands due to a lack of detailed molecular information on the OTR, making this receptor full of untapped potential as a therapeutic target. WAY-267,464 is among the first-generation non-peptide ligands used as a valuable research agent [13, 25-31]. Interestingly, Jorgensen et al. found that methylation of its resorcinol moiety removed the agonist activity, creating a WAY-267,464 derivative (hereby referred to as WAY-Methylated) that acts as an OTR partial antagonist [13]. This dramatic activity change due to a single methylation raises many interesting questions. While pharmacological data has been collected [13, 25-29, 31], there have been no binding poses or receptor conformational changes reported to aid in answering these questions. Limited

mutagenesis studies on the OTR have revealed a list of key residues important for ligand binding as well as some evidence that agonist activity is increased with hydrophobic interactions at the N-terminus [6, 18, 32, 33]. Homology model mapping and molecular docking studies have also been used to discover such key residues; however, these studies have focused on peptides or various small ligands not specific to the OTR [4, 34]. Development of non-peptide OTR ligands is further hindered by and the lack of a crystal structure as well as details on molecular interactions. Here, docking with and without a positional constraint were used to explore the OTR orthosteric pocket. The docked complexes were then relaxed and submitted to a 200 ns MD simulation using an OPLS3 force field [35]. After computation of MM-GBSA binding energies for more accurate ranking of the binding poses for each ligand, the preferred configuration for each ligand-complex was further subjected to an additional 2 µs MD simulation. Differences ligand binding patten and the receptor conformational changes were thoroughly analyzed. Furthermore, key receptor-ligand interactions were compared with the experimental and computational findings in the literature.

2. Methods

2.1. Homology modeling and system Set up

The human OTR FASTA sequence (P30559) (Fig. S1) file was retrieved from the Uniprot database [36]. The Structure Prediction Wizard of Maestro [37, 38] was used to build a homology model of the human OTR, using the crystal structure of the nociception receptor in complex with antagonist DGV (PDB ID: 5DHG) [39] as a template. The crystal structure of nociception receptor with antagonist DGV was found to have the highest similarity score of 193.0, 29% identities, and 43% positive residues (Fig. S2). The receptor was oriented in membrane using the OPM web server [40] and then prepared using Maestro's Protein

Preparation Wizard [41]. The protein was preprocessed to assign correct bond orders, add hydrogen atoms, create disulfide bonds, and to delete water beyond 5 Å from hetero groups. The charge state of the titratable residues was optimized using PROPKA at a pH of 7. A restrained minimization was done to relax the protein using an OPLS3 force field [35]. Two dimensional (2D) structures of DGV, WAY-267,464, and WAY-Methylated were built in Maestro. The structures were then converted to three dimensional (3D) models. Epik, a tool based on accurate methodologies from Hammer and Taft [41], was used to generate the proper ionization state of each ligand. The lowest tautomeric state for each ligand structure was selected and minimized to relax the ligands to a best fit structure. Lastly, a geometry optimization was performed using quantum mechanics methods in Jaguar.

2.2. Molecular docking

To investigate the accuracy of molecular docking with larger ligands, the co-crystallized ligand (DGV) of the template structure was docked back to its original binding position in the crystal structure. Glide docking with default parameters was unable to reproduce the original binding pose. Glide with a positional constraint was able to reproduce the original orientation and position of DGV seen in the crystal structure (Fig. S3). The atoms used to create the positional constraint for DGV are shown in Fig. S4A.

2.2.1. Docking without constraint

The fully prepared merged protein-ligand complex was used to create the receptor grid file. The active binding site of the OTR was defined using the center of the ligand. The grid file was generated using a van der Waals scaling factor of 1 and a partial charge cutoff of 0.25. The

prepared WAY-267,464 and WAY-Methylated were docked into the generated grid of the protein receptor using an OPLS3 force field and their docking scores were calculated using an XP scoring function [35]. The default settings were used as parameters of the scoring function: ligand sampling was flexible, with sample nitrogen-inversions, same ring conformations, and bias sampling of torsions for amides which only penalized nonpolar conformations and added Epik state penalties to the docking score [42, 43]. The docking results indicated that the two ligands bound in slightly different binding poses. To check for the possibility of an alternative binding pose in which the ligands were flipped, the following constrained docking was performed.

2.2.2 Docking with constraint

A constrained receptor grid file was generated in the same manner as in the unconstrained ligand docking; the only difference was that a positional constraint was used. WAY-267,464 and WAY-Methylated were docked with the same positional constraint (PC) as DGV. The atoms used to create the positional constraint for WAY-267,464 and WAY-Methylated are shown in Fig. S4B. The center of the ligand was used to define the center of the active site of the receptor. The positional constraint used a cutoff distance of 1.0 Å. The grid file was generated using a van der Waals scaling factor of 1 and a partial charge cutoff of 0.25. The prepared WAY-267,464 and WAY-Methylated ligands were constrained-docked into the generated grid file of the receptor using an OPLS3 force field and their docking scores were calculated using an XP scoring function [35]. The parameters of the scoring function were the same as in the unconstrained docking.

2.3. Molecular dynamics simulation

2.3.1. Molecular dynamics simulation system setup

The four prepared receptor-ligand complexes from the XP docking and XP docking with a positional constraint were used to construct molecular dynamics simulation systems. The complexes were placed in a predefined POPC (300 K) lipid membrane model [44] and aligned in the membrane according to the helices in the transmembrane region. It was then solvated in an orthorhombic water box with a buffer distance of 8 Å using a predefined SPC water model [45]. A 0.15 M NaCl salt concentration was added to neutralize the system. The systems were built with an OPLS3 force field using Desmond System Builder in Maestro on a Linux operating system [35].

2.3.2. Relaxation and production runs

The relaxation/ minimization and production runs of the four set-up systems were done using the Desmond module. Each system was relaxed using the default eight-step relaxation protocol for membrane proteins [46]: (1) Minimization with restraints on heavy solute atoms.

(2) Minimization without any restraints. (3) Simulation with a heat transition from 0 to 300 K, a water barrier, and gradual restraining. (4) Simulation under NPT (Constant number of particles, constant pressure of 1 bar, and constant temperature at 300K) condition with a water barrier and heavy atoms restrained. (5) Simulation under NPT condition with additional equilibrations of both lipids and solvents. (6) Simulation under NPT condition with heavy atoms annealing from 10 to 2 kcal/mol. (7) Simulation under NPT condition with Cα atoms restrained at 2 kcal/mol. (8) Simulation under NPT conditions without restraints for 1.5 ns.

Following this relaxation process, each of the four systems was submitted to a production run of 200 ns in NPT ensemble using the default protocol. After analyzing these preliminary MD simulation results, the preferred configuration of each protein-ligand complex was re-submitted to a 2 µs-production run. The preferred configuration for WAY-267,464 was the XP-docked complex, while that of WAY-Methylated was the PC-docked complex. In all these simulations, the temperature was controlled by the Nosé-Hoover chain coupling scheme [47] with a coupling constant of 1.0 ps, the pressure was controlled by the Martyna-Tuckerman-Klein chain coupling scheme [47] with a coupling constant of 2.0 ps. All bonds connected to hydrogen atoms were constrained by applying M-SHAKE [48] and enabling a 2.0 fs time-step within the simulations. Long-range electrostatic interactions were analyzed using the k-space Gaussian split Ewald method [49] under periodic boundary conditions, with a charge grid spacing of ~ 1.0 Å and a direct sum tolerance of 10⁻⁹. The short-range non-bonded interactions had a cutoff distance of 9 Å. The long-range van der Waals interactions were based on a uniform density approximation. To condense the computation, a r-RESPA integrator [50] was used to calculate non-bonded forces, where every step of the short-range forces were updated and every three steps the longrange forces were updated. The trajectories obtained from the simulations were saved at 50.0 ps intervals for analysis.

2.3.3. Simulation interaction diagram (SID) analysis

The Desmond SID tool in Maestro was used to compute the Root-Mean-Square Deviation (RMSD), the Root-Mean-Square Fluctuation (RMSF), the Secondary Structural Elements (SSE), and the residue-ligand interactions and contacts throughout the course of the simulation. To ensure the convergence of each of the MD simulations, the protein Cα and ligand RMSD plots

obtained from the SID analysis were analyzed. A relatively flat plot indicates that a steady state was reached. The last 50 ns of each shorter simulation show little deviation, indicating convergence (Fig. S5). The last 500 ns of each longer simulation show minor deviation, indicating convergence in these as well.

2.3.4. Trajectory clustering analysis

The Desmond clustering tool [51] was used to group the complex structures from the last 50 ns of each of the shorter MD trajectories and the last 500 ns for the longer trajectories. The backbone RMSD matrix was used as the structural similarity metric. The hierarchical clustering with average linkage, using a 2.5 Å merging distance cutoff was used. The structure with the most neighbors in the structural family, known as the centroid structure, was chosen to represent each structural family. The most abundant centroid structures of the populated structural families were extracted and analyzed further.

2.4. Binding energy calculations and decompositions

The surface-area-based Generalized Born model [52, 53] with an implicit membrane solvation model (VSGB 2.0) [54] was used to calculate ligand-binding affinities on the frames obtained in the last 50 ns (short) and 200 ns (extended) of each MD simulation. The implicit membrane is a slab-shaped region with a low dielectric constant between 1 and 4, and the regions to exclude from the membrane were assigned with the solvent (water) dielectric constant of 80. An OPLS3 force field and the default Prime procedure were used for the MM-GBSA calculation [55]. The OPLS3 force field employs a CM1A-BCC-based charge model based on a combination of Cramer-Truhlar CM1A charges [56] with an extensive parameterization of bond

charge correction terms (BCC). This default procedure first minimizes the receptor alone, then the ligand alone, and then receptor-ligand complex. The MM-GBSA binding free energy for each system was calculated from three separate simulations: ligand only, receptor only, and the receptor-ligand complex, using equation 1. There are four components in equation 2: van der Waals interaction energy (VDW), hydrophobic interaction energy (SUR), electrostatic interaction (GBELE), and the change of the conformation energy for receptor and ligand. These terms were calculated using equations 3 and 4.

$$\Delta E = E_{complex} - E_{rec\ free} - E_{lig\ free} \tag{1}$$

$$\Delta E = \Delta E_{vdw} + \Delta E_{SUR} + \Delta E_{GBELE} + \Delta E_{comformation}$$
 (2)

$$\Delta E_x = E_{x_complex} - E_{x_rec_complex} - E_{x_lig_complex}$$
, $x = vdw$, sur and gbele (3)

$$\Delta E_{Comformation} = E_{rec_complex} + E_{lig_complex} - E_{rec_free} - E_{lig_free}$$
 (4)

Although the MM-GBSA scoring function lacks the solute conformational entropy contribution, which results in higher negative values when compared to the actual values, it has proven to be an extremely useful tool in ranking a drug's ability to target a receptor, when it is used to rank different drugs targeting receptors with comparable entropy values [57]. Previous studies, including the testing with 1,864 crystal complexes, have shown that MM-GBSA is a powerful tool in ranking ligands [58-62].

2.5. Dynamical network model

Using the NetworkView plugin [63] in VMD [64], the full trajectory of each system was used to generate a dynamic network model, defined as a set of nodes connected by edges [63]. For each system, a contact map which added an edge between nodes whose heavy atoms interacted within a cutoff of 4.5Å for at least 75% of the MD simulation time, was generated.

This edge distance was derived from pairwise correlations [63] using the program Carma [65]. The probability of information transfer across a given edge is calculated using the following equation:

$$C_{ij} = \frac{\langle \Delta \overrightarrow{r_i}(t) \cdot \Delta \overrightarrow{r_j}(t) \rangle}{(\langle \Delta \overrightarrow{r_i}(t)^2 \rangle \langle \Delta \overrightarrow{r_j}(t)^2 \rangle)^{1/2}}$$
$$\Delta \overrightarrow{r}(t) = \overrightarrow{r_i}(t) - \langle \overrightarrow{r_i}(t) \rangle$$

The edges are weighted (w_{ij}) between any two nodes i and j and is calculated as follows: $w_{ij} = -\log(|C_{ij}|)$. The weight of the edge represents the probability for transfer of information across the edge between the two nodes—thicker edge denotes a higher probability of information transfer.

Each of the generated networks was then further grouped into subnetworks, referred to as communities, based on groups of nodes with stronger and more frequent connections to each other using Girvan-Newman algorithm [66]. The critical nodes that connect communities to one another were identified. Using molecular switch information, an optimal communication path was generated between the ligand binding site node and molecular switch residue.

3. Results

3.1. The positional constraint produced opposite ligand orientations when compared to their original binding pose

From the standard XP docking, WAY-267,464 was positioned so that the head group (resorcinol moiety) was located towards the central region of the receptor, while the tail group (three aromatic rings) was located between transmembranes (TM) 3 and 5. When it was PC-docked, its orientation flipped so that the head group was positioned between TMs 4 and 5, and the tail group was in the central region. The docking scores were -6.306 kcal/mol and -6.614

kcal/mol for XP and PC docking, respectively (**Fig. 1**). The XP docking of WAY-Methylated bound the ligand with both the head and tail groups facing down towards the binding pocket in a kinked vertical fashion not seen in either of the docking positions for WAY-267,464. The central region of the ligand was located closer to the extracellular region outside of the receptor. When WAY-Methylated was docked with positional constraint, the ligand flipped the orientation of its head and tail groups and straightened out the central region such that it was no longer vertically kinked. The docking scores for XP- and PC-docked WAY-Methylated were -6.514 kcal/mol and -8.804 kcal/mol, respectively. The PC-docked ligands resulted in the central portion of either ligand to bind deeper within the binding pocket than the XP-docked ligands (Fig. S6).

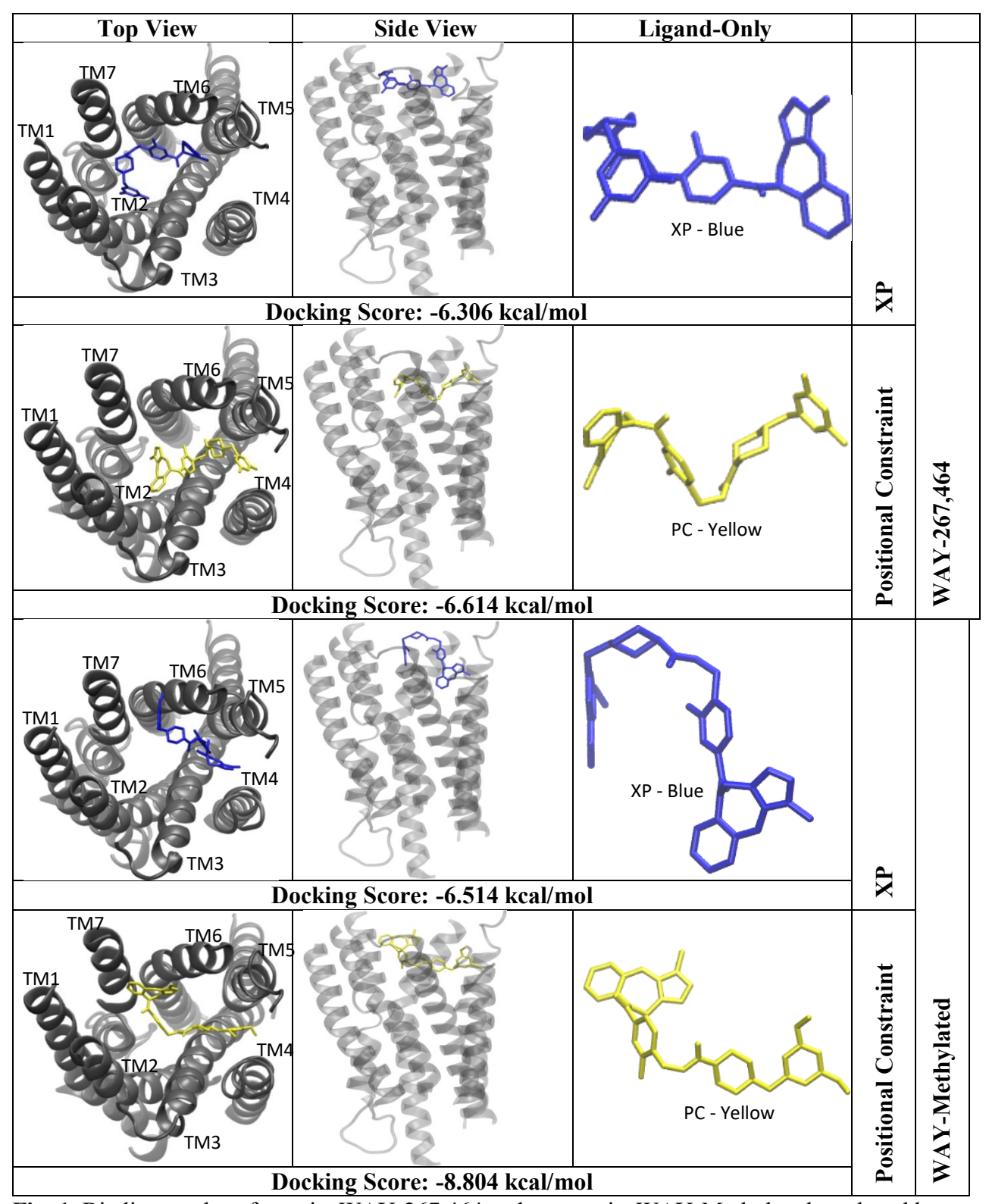


Fig. 1. Binding modes of agonist WAY-267,464 and antagonist WAY-Methylated produced by standard extra-precision (XP) Glide docking and docking with position constraints (PC).

3.2. MM-GBSA binding energy data revealed the preferred docking method for each ligand To rank the receptor-ligand binding pose, we performed MM-GBSA binding energy calculations [67] on the four systems as described in the method section. The results from the initial short 200 ns MD simulations are presented in **Table 1**. Interestingly, standard docking produced the most stable binding pose of WAY-267,464. While docking scores are not solely used to determine stability, it is rather interesting that the MM-GBSA values are so dramatically different when the docking scores were relatively close. The MM-GBSA binding energy of XP-docked WAY-267,464 was -128.8 kcal/mol. The most favorable binding pose of WAY-Methylated was the PCdocked pose. Of all the four systems, the PC-docked WAY-Methylated was found to have the largest MM-GBSA binding energy score of -156.0 kcal/mol. The preferred configuration of each complex (XP-docked for WAY-267,464 and PC-docked for WAY-Methylated) was then submitted to 2 µs MD simulation to ensure accurate binding data and ligand-receptor interactions were collected. The results of the 2 μs MD simulations are presented in **Table 2**. The MM-GBSA binding energy values for each system were similar to those obtained in the previous shorter simulations. The MM-GBSA binding energy score for WAY-267,464 and WAY-Methylated for the 2 μs MD simulations were -116.9 kcal/mol and -152.8 kcal/mol—both are slightly lower than the scores for the preliminary shorter simulations. The experimental binding affinity (IC50) values of WAY-267,464 and WAY-Methylated for the OTR and V_{1A}R receptors are also shown in **Table 3**.

Table 1. MM-GBSA values computed for the last 50 ns of 200 ns MD simulation.

Activity	Ligand	Docking Method	Docking Score (kcal/mol)	MM-GBSA (kcal/mol)
Agonist	WAY-267,464	XP	-6.3	-128.8 <u>+</u> 9.3
		PC	-6.6	-98.4 <u>+</u> 8.6
Antagonist	WAY-Methylated	XP	-6.5	-136.8 <u>+</u> 10.4
		PC	-8.1	-156.0 <u>+</u> 10.1

Table 2: The most abundant cluster percentage of the 2 μ s MD simulation with the MM-GBSA value computed for the last 200 ns.

Activity	Ligand	Docking Method	Cluster Abundance (%)	MM-GBSA (kcal/mol)
Agonist	WAY-267,464	XP	30.5	-116.9 <u>+</u> 13.0
Antagonist	WAY- Methylated	PC	96.4	-152.8 <u>+</u> 10.2

Table 3. Experimental binding affinities of WAY-267,464 and WAY-Methylated for the OTR and $V_{1A}R$ receptors. Units are shown in nM [13].

Receptor		OTR				V _{1A} R		
Activity	Ligand	\mathbf{K}_{i}	EC50	IC50	\mathbf{K}_{i}	EC50	IC ₅₀	
Agonist	WAY- 267,464	230 <u>+</u> 31	420 <u>+</u> 59	> 10,000	27 <u>+</u> 3	>10,000	613 <u>+</u> 206	
Antagonist	WAY- Methylated	801 <u>+</u> 139	> 10,000	4129 <u>+</u> 645	62 <u>+</u> 21	>10,000	1113 <u>+</u> 180	

Reference number 13 in the text

3.3. The MD simulations significantly relaxed the complex structures

The protein and ligand Root-Mean Square Deviation (RMSD) plots over 200 ns for the four systems can be found in the Supporting Information (Fig. S5), while the RMSD plots for the preferred configuration for each ligand over 2 µs are shown in **Fig. 2**. For the WAY-267,464

complex, the initial conformational adjustment occurred over the first 1000 ns, followed by stable RMSDs of the receptor and ligand over the remaining simulation time. For the WAY-Methylated complex, the initial conformational adjustment occurred over the first 750 ns, followed by stable RMSDs of both the receptor and ligand over the remaining simulation time. Each system was sufficiently relaxed after the initial conformational adjustment period. The MD simulation-derived ligand-OTR complexes maintained the pose scaffold of the docked complexes, further validating our MD simulation methodology (Fig. S7). The fact that WAY-267,464 is an agonist and that WAY-Methylated is an antagonist, the two different binding poses observed may be consistent with their opposing activities.

Trajectory clustering [51] identified the most abundant representative structure for each system (Fig. S8). The percentages of the most populated cluster for WAY-267,464 and WAY-Methylated were 30.5% and 96.4%, respectively. To facilitate the comparison between the two complexes, we superimposed their representative structures (Fig. 3). The most abundant XP-docked WAY-267,464 binding pose resulted in the head group binding closer to the N-terminal and the tail group binding deeper into the OTR binding pocket. The most abundant PC-docked WAY-Methylated binding pose resulted in the tail group binding closer to the N-terminal instead, while the head group bound more superficially within the binding pocket.

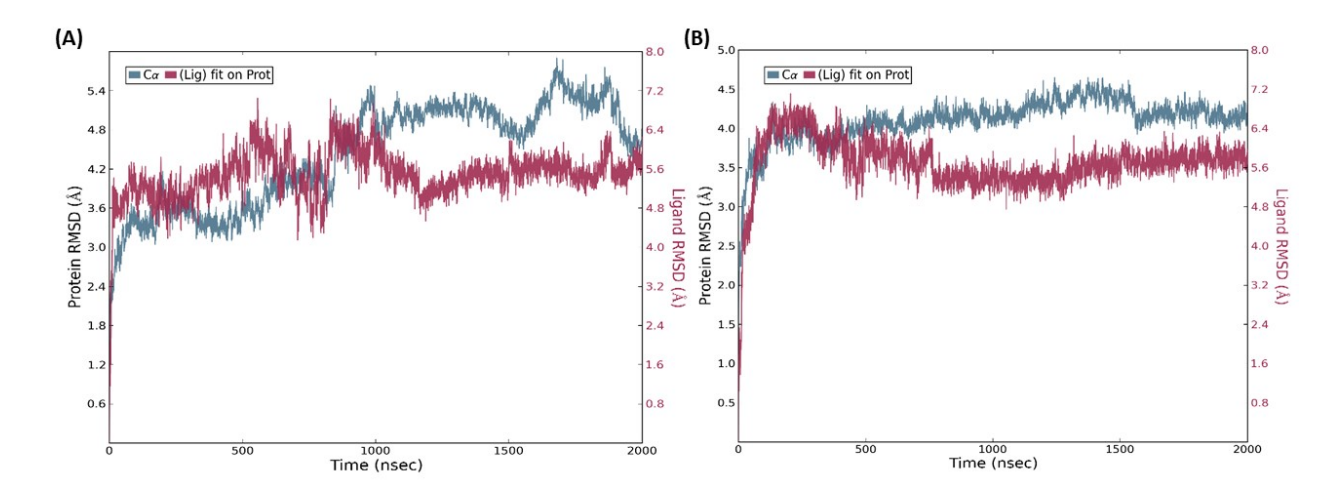


Fig. 2. Root Mean Square Deviation (RMSD) of the long 2 μs simulations of WAY-267,464 (A) and WAY-Methylated (B) complexes. Protein Cα-RMSD is measured using the initial frame as reference, while the ligand RMSD refers to in-place RMSD of ligand when protein is aligned.

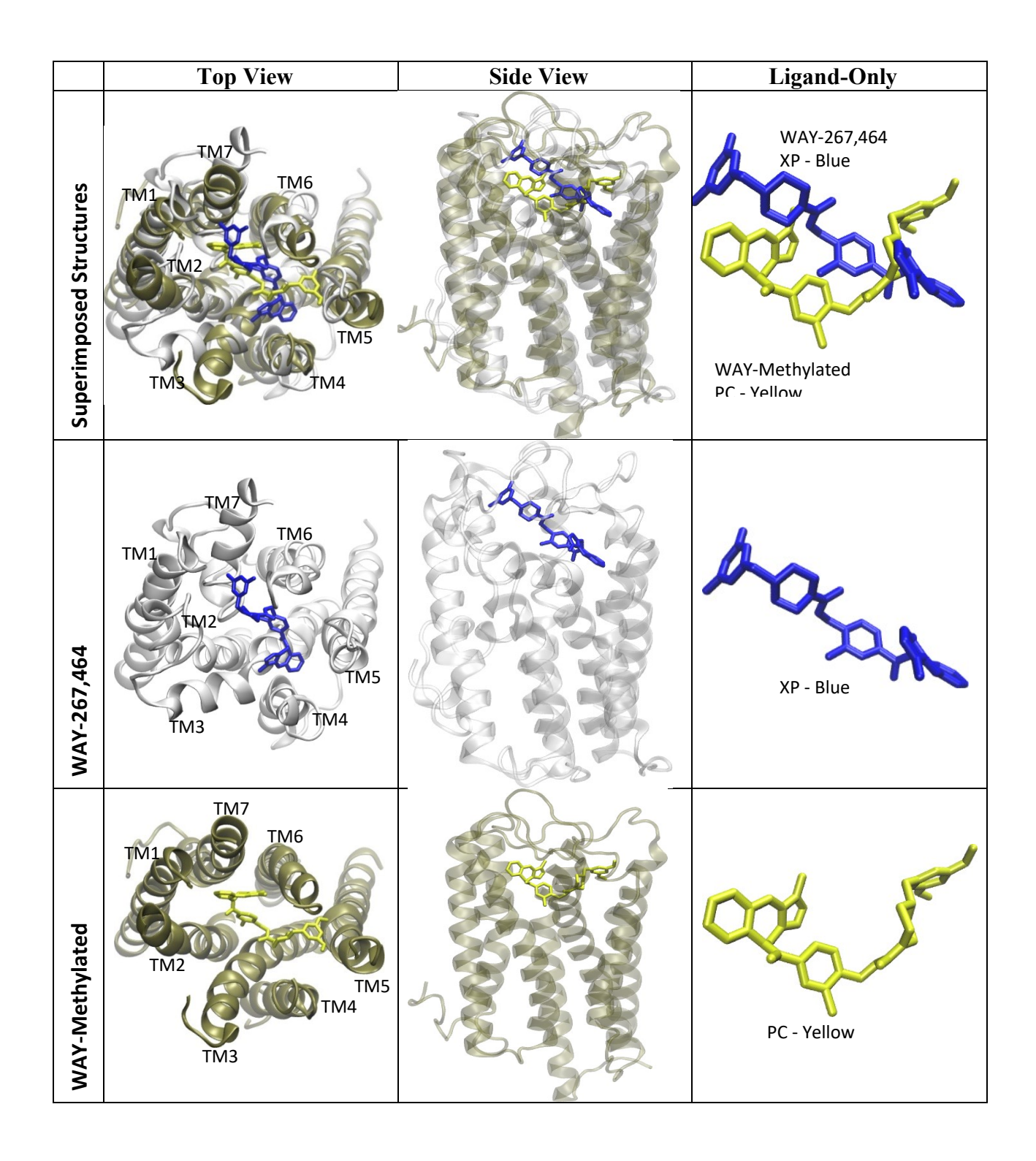


Fig. 3. 3D structural comparison of the most abundant clusters from the 2 μ s MD simulations for the WAY-267,464 and WAY-Methylated systems.

The protein-ligand interactions persisting more than 30% of the simulation and their frequencies over 200 ns time period are given as Figs. S9 and S10, respectively, while the corresponding protein-ligand interactions and frequencies for the 2 µs simulations are presented in Fig 4, with the top interacting residues for each of the simulations given in Table 4. All the interacting residues in this table were assigned a genetic number for OTR. There are seven key residues reported in the literature to interact with the ligands and these are Trp99^{2.64}, Lys116^{3.29}, Gln119^{3.32}, Ile204^{5.43}, Tyr209^{5.47}, Phe291^{6.51}, and Gln295^{6.55} [3, 4, 8, 18, 33]. Consistent with the MM-GBSA binding score, XP-docked WAY-267,464 interacted with more key residues than the PC-docked system. The significant OTR/ WAY-267,464 interactions from the 2 µs simulations involved five of the seven key residues in TMs 2, 3, 5, and 6. Trp99^{2.64} interactions consisted of a mixture of hydrophobic interactions, hydrogen bonds, and water bridges. Lys116^{3.29} interacted 38% of the simulation time with the tail group (the end located deeper in the binding pocket) of WAY-267,464 and with a water molecule packed within this region. Gln295^{6.55} interacted 32% of the simulation time with the central carboxyl oxygen (the one closest to the tail group) of WAY-267,464 and with a water molecule packed within this region as well. The interactions between the ligand and Lys116^{3,29}/ Gln295^{6,55} mainly consisted of water bridges and hydrogen bonding. The significant OTR/WAY-267,464 interactions involved all seven of the key residues in TMs 2, 3, 5, and 6. Consistent with MM-GBSA binding energy values for the PC-docked WAY-Methylated system, all these residues were found to interact with WAY-Methylated. For WAY-267,464, the highest interaction fractions of these residues were from Lys116^{3.29} and Gln295^{6.55}. Lys116^{3.29} interacted 66% of the simulation time with the central aromatic ring of WAY-Methylated. Gln295^{6.55} interacted 84% of the simulation time with the central NH group of the ligand. However, these interactions between WAY-Methylated and Lys116^{3.29}/Gln295^{6.55}

mainly consisted of hydrophobic contacts and hydrogen bonds, rather than with water bridges as was seen in WAY-267,464. Ile313^{7,36} was another residue with a large hydrophobic interaction fraction reported for WAY-Methylated (**Fig. 4**).

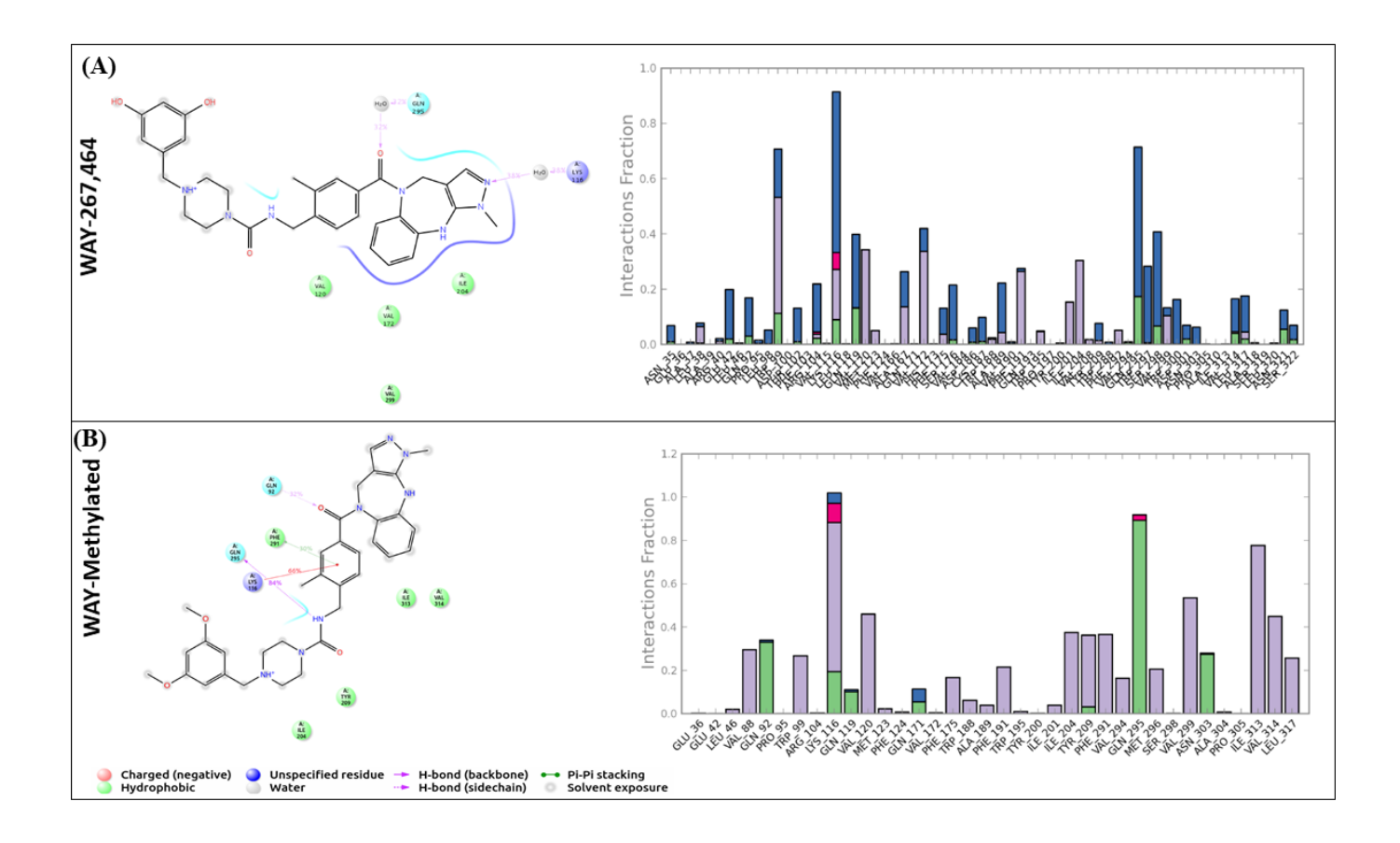


Fig. 4. Detailed residue-ligand interactions that were present in over 30% of the 2 μs MD simulations and protein residue-ligand contact histograms for WAY-267,464 (A), and WAY-Methylated (B).

Table 4. Residues of the OTR interacting with WAY-267,464 and WAY-Methylated with an observed interaction fraction above 10% of simulation time. Red residues represent key residues found in literature.

Con No	WAY-267,464			WAY-Methylated		
Gen No.	Short XP	Short PC	Long XP	Short XP	Short PC	Long PC
1.33	ARG40					
1.35	GLU42		GLU42			
2.53						VAL88
2.57			GLN92		GLN92	GLN92
2.60		PRO95				
2.64	TRP99 ⁵		TRP99 ⁵		TRP99 ⁵	TRP99 ⁵
E1			THR102			
E1	ARG104		ARG104			
3.28		VAL115				
3.29	LYS116 ⁴⁻⁵	LYS116 ⁴⁻⁵	LYS116 ⁴⁻⁵	LYS116 ⁴⁻⁵	LYS116 ⁴⁻⁵	LYS116 ⁴⁻⁵
3.32	GLN119 ³⁻⁵	GLN119 ³⁻⁵	GLN119 ³⁻⁵		GLN119 ³⁻⁵	GLN119 ³⁻⁵
3.33			VAL120		VAL120	VAL120
3.36	MET123					
4.56			ALA167			
4.61		GLN171				GLN171
4.62	VAL172		VAL172	VAL172		
4.65	PHE175		PHE175	PHE175	PHE175	PHE175
E2	11121,0		SER176	1112170	1112170	11121,0
E2	ASP186		SEITH, 0			
E2	CYS187		CYS187			
E2	C15107	TRP188	015107	TRP188		
E2		ALA189	ALA189	ALA189		
E2		PHE191	PHE191	PHE191	PHE191	PHE191
E2	TRP195	TILLIJI	11112171	TRP195	TILLIJI	11111171
5.39	1Ki 195			TYR200		
5.40	ILE201		ILE201	ILE201		
5.43	ILE201 ILE204 ³⁻⁴		ILE201 ILE204 ³⁻⁴	ILE201 ILE204 ³⁻⁴	ILE204 ³⁻⁴	ILE204 ³⁻⁴
5.43 5.47	ILE204		1LL204	TYR209 ³⁻⁴	TYR209 ³⁻⁴	TYR209 ³⁻⁴
6.51		PHE291 ¹⁻⁵		1 1 K209	PHE291 ¹⁻⁵	PHE291 ¹⁻⁵
6.52	PHE292	PHE291			PHE291	PHE291
	PHE292				3741 204	VAT 204
6.54	GLN295 ²⁻⁵	GLN295 ²⁻⁵	GLN295 ²⁻⁵	GLN295 ²⁻⁵	VAL294 GLN295 ²⁻⁵	VAL294 GLN295 ²⁻⁵
6.55	GLN29323	GLN293	GLN29323	GLN29323		
6.56			TDD207	TDD207	MET296	MET296
6.57	GED200	GED200	TRP297	TRP297		
6.58	SER298	SER298	SER298	SER298	1741.000	1741.000
6.59	VAL299	VAL299	VAL299	TDD000	VAL299	VAL299
6.60			TRP300	TRP300		
6.61		ASP301				
E3		nn		ASN303		ASN303
E3		PRO305		PRO305		
7.36				ILE313	ILE313	ILE313
7.37	VAL314	VAL314	VAL314		VAL314	VAL314
7.40	LEU317	LEU317	LEU317		LEU317	LEU317
7.45			ASN321			

¹: Reference number 41 in text

²: Reference number 18 in text

³: Reference number 3 in text

^{4:} Reference number 8 in text

⁵: Reference number 4 in text

3.4. Secondary structure changes and structural fluctuations

To investigate the secondary structure of the receptor in each ligand complex, the most abundant secondary structures that each individual protein residue experienced over the trajectory and time evolution are shown in **Fig. 5**. Some particularly notable changes include a gain of helical structure in TM2, a non-kinked TM3, a complete loss of β -strands in E2, a non-kinked TM6, and a gain of helical structure/ less kinks in TM7 observed in the WAY-Methylated complex when compared to the WAY-267,464 complex. The β -strand percentage abundance dropped from 1.17% to 0.07%, while the α -helix percentage abundance increased from 46% to 61%, in the WAY-267,464 complex and WAY-Methylated complex, respectively. These subtle changes in receptor conformation might be closely linked to the activity difference displayed by the ligands.

The protein $C\alpha$ RMSF values for both ligand complexes are shown in **Fig. 6A.** We observed the general expected trend that the most rigid parts of the protein receptor (i.e. transmembrane helices) exhibit lower RMSF values while the more flexible parts (i.e. N/C terminals regions and intra/extracellular loops) exhibit higher RMSF values. In addition, some subtle differences were identified for each ligand-OTR complex. Most notably, WAY-267,464 induced a higher intracellular loop 3 (I3) fluctuations than WAY-Methylated did by 5.65 Å. Given the different activities of each ligand on the OTR, these slight dynamic differences may contribute to the different responses by modulating the interaction between the OTR and the down-stream signal transduction proteins, such as G-proteins or β -arrestin [1, 5, 15, 17-19, 23, 24, 68, 69].

The ligand RMSF over time for each complex are shown in **Fig. 6B** with the mean values for each ligand listed in Table S1. WAY-Methylated displayed less structural fluctuation. In fact,

WAY-Methylated had less than half the mean fluctuation value as WAY-267,464 (1.05 Å vs 2.67 Å, respectively). WAY-267,464 showed more structural fluctuation, mainly in the head group (resorcinol moiety). Thus, it can be assumed that the WAY-267,464 ligand binds in a more flexible and less stable binding pose than does WAY-Methylated. This is consistent with our MM-GBSA binding energy data showing the WAY-Methylated to bind stronger to the OTR than WAY-267,464.

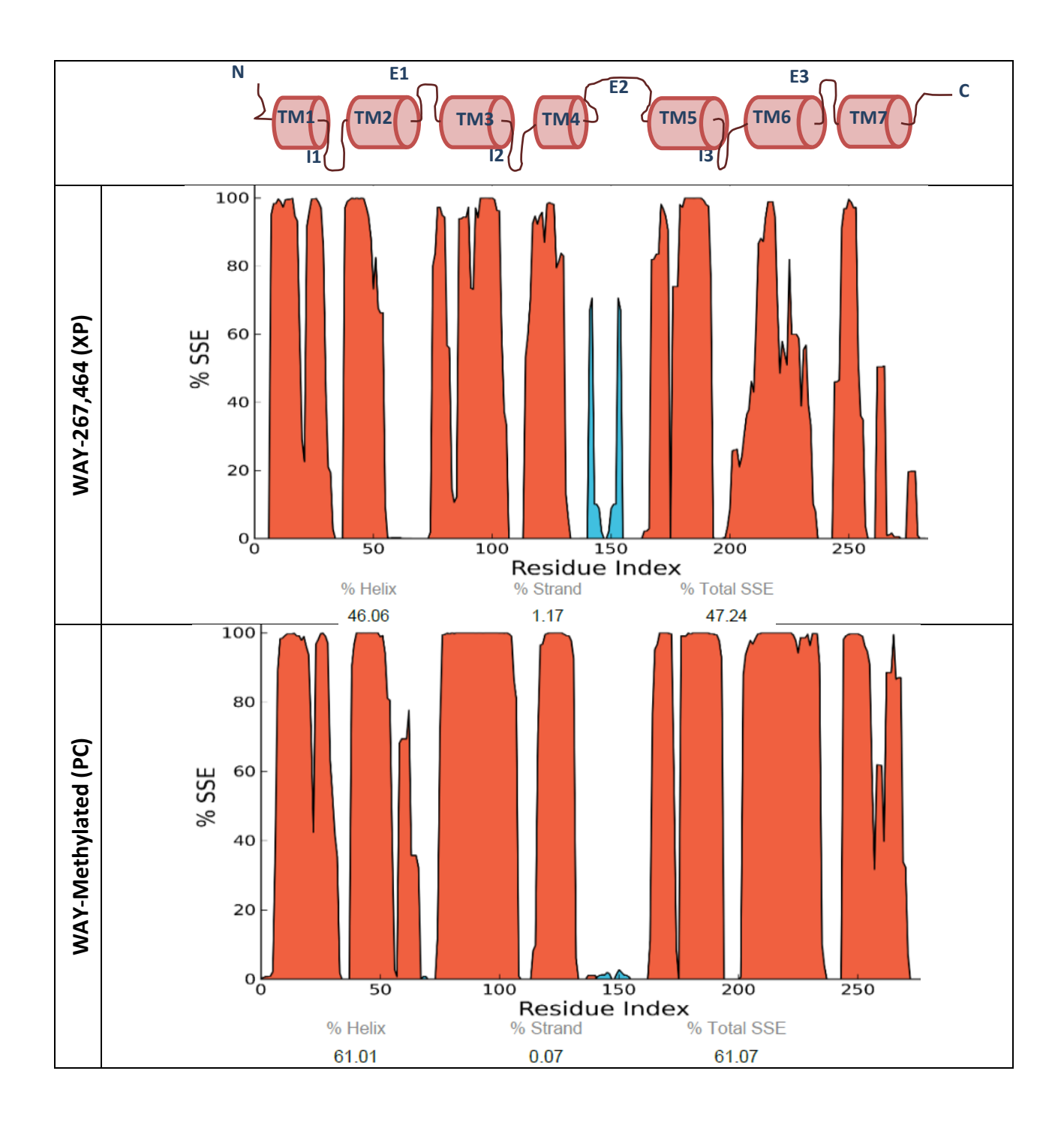


Fig. 5. Comparison of the Secondary Structural Elements (SSE) at each protein residue for the 2 μs MD simulations for the WAY-267,464 and WAY-Methylated complexes. Overall SSE percentage contribution is annotated.

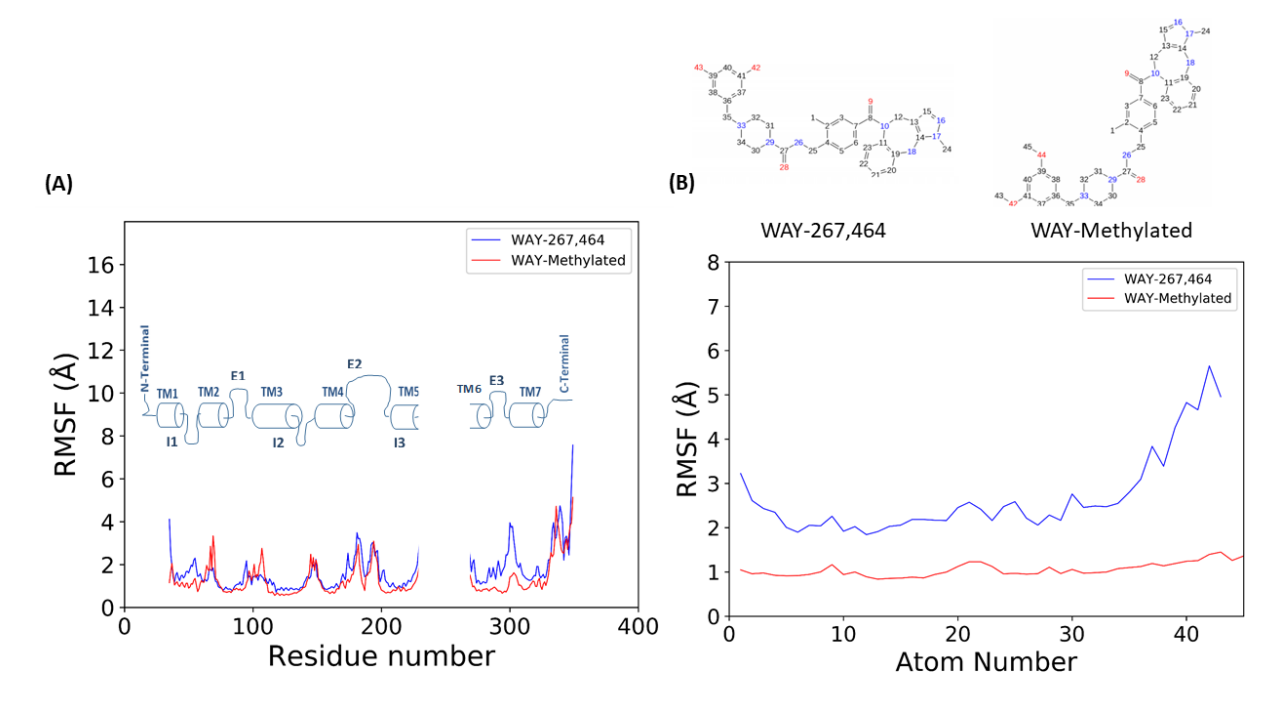


Fig. 6. Protein Cα RMSF diagram for 2 μs MD simulations for each of the complexes (A). The corresponding ligand RMSF diagram with ligand structures with annotated atom numbers (B).

3.5. Comparison of the molecular switches between WAY-267,464 and WAY-Methylated suggests partial activation of the receptor by WAY-267,464.

Molecular switches are a set of noncovalent interactions stabilizing protein structure, and whose disruption or formation due to conformational changes respectively lead to activation or inactivation of the receptor. Brian Kobilka adds that they are non-covalent interactions that exist in the basal state of a GPCR [70]. These switches can be compared by examining the conformation of OTR complexed with the agonist and antagonist (**Fig. 7**). In this study, the distance of residues was measured at the tyrosine toggle switch, transmission switch, and the ionic lock switch for WAY-Methylated and WAY-267,464 and was compared to the data from a study on class A GPCR by Trzaskowski *et al.*[71] For the representative structures obtained from

trajectory clustering, the transmission switch showed a distance of 3.9 Å at T273:CA, and 4.7 Å at W297 between agonist and antagonist structures. This distance appears to be similar to that shown by Trzaskowski et al. [71], suggesting partial activation. The tyrosine toggle switch showed a moving distance of 4.2Å at Y329 between the agonist WAY-267,464- and antagonist WAY-Methylated-bound structures. Fig. 7F shows that TM7 has unraveled whereas the tyrosine toggle switch retained its helical form. This suggests that the oxytocin toggle switch may have been disrupted. The ionic lock showed a moving distance of 9.9 Å at D136:CG – K270:NZ on the antagonist and 11.7 Å at D136:CG – K270:NZ on the agonist (**Table 5**). The large distance indicates that the salt bridge was already broken in both systems (Fig. S11A). Thus, the ionic lock in the WAY-Methylated bound system does not follow the format of inactivation. In addition, when compared to the receptors used in Trzaskowski et al. [71] the ionic lock in the OTR shows conservation at positions 3x49, 3x50, and 5x58, (D,R,Y respectively) but does not show conservation at position 6x30 (K on oxytocin, E on Trzaskowski et al. [71]). The tryptophan toggle (W297) dihedral angles profile showed subtle difference between the two systems until 300 ns, then synchronized for the remaining time of the simulation (Fig. S11B). The tyrosine toggle switch at Tyr329 in the agonist WAY-267,464-bound system showed a complete flipping from negative to positive dihedral angles at around 500 ns whereas no remarkable changes were seen in the WAY-Methylated system (Fig. S11C).

Table 5. Conserved molecular switches within OTR and their respective distances between residues involved.

UNC9975/Dopamine	Residues	Distance (Å)
Tyr Toggle (NPXXY)	Y329 ¹ -Y329 ²	4.2
Transmission	T273 ¹ :CA-T273 ² :CA	3.9
(CWXP)	W297 ¹ -W297 ²	4.7
Ionic Lock	D136:CG ¹ -K270:NZ ¹	9.9
(DRY)	D136:CG ² -K270:NZ ²	11.7

OTR-WAY-Methylated complex structure

²OTR-WAY264,464 complex structure

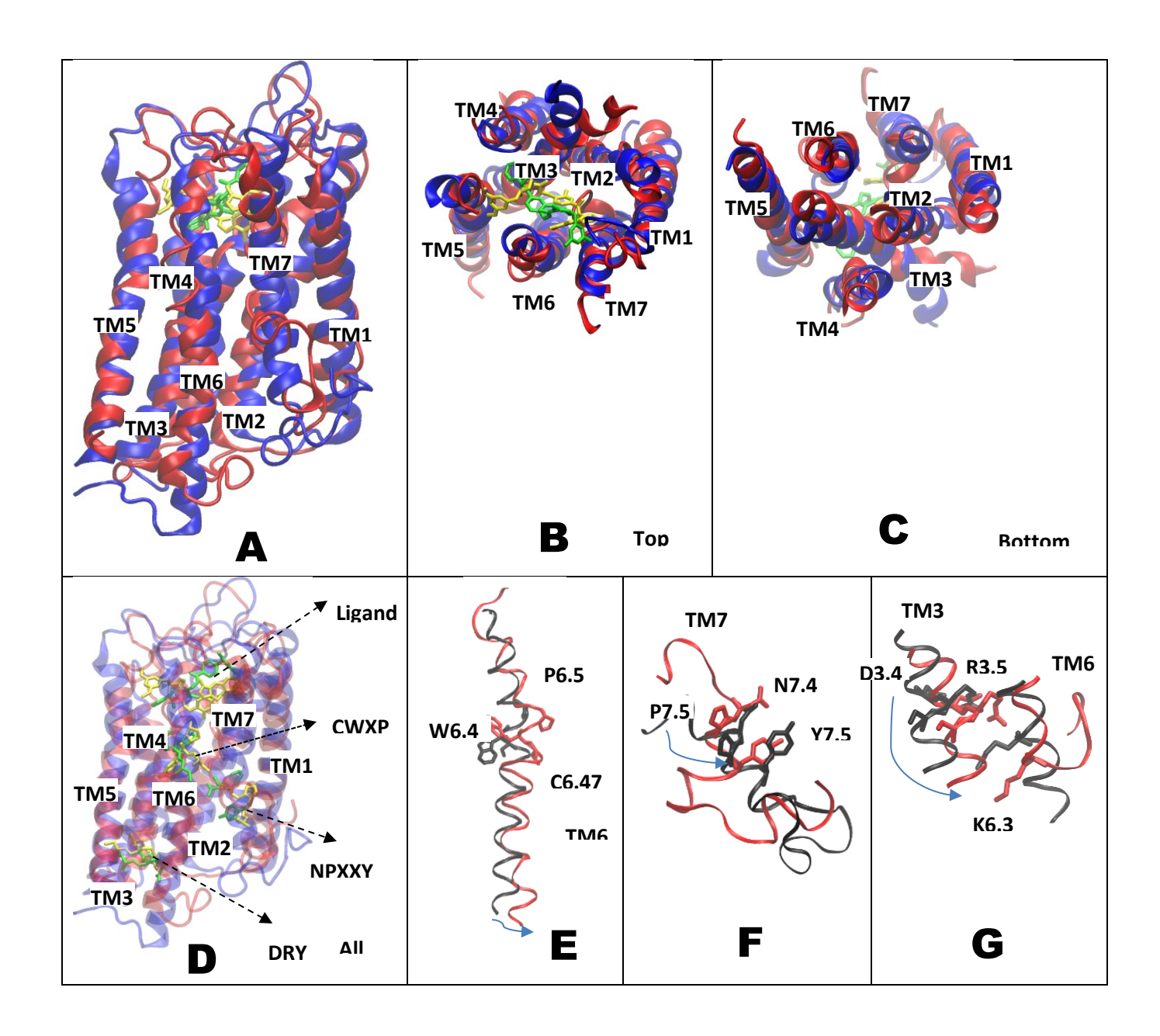


Fig. 7. WAY-Methylated and Way-267,464 ligands in complex with OTR (WAY-Methylated/OTR: blue/yellow; WAY-267,464/OTR: green/red) (**A**). Top view (**B**). Bottom view (**C**). All switches overlapped aligned with structure of Dopamine/D2 (**D**). Transmission switch (CWXP) (**E**). Tyrosine toggle switch (NPXXY). (**F**). Ionic lock Switch (DRY)(**G**). **E-G**: UNC9975/D2: black; Dopamine/D2: red.

3.6. The dynamic network model identified remarkable differences between the WAY-267,464 and WAY-Methylated bound systems

To understand differences in the signal transmission pathways, unweighted and weighted network models of WAY-267,464- and WAY-Methylated-bound systems were generated as described in the method section. The weighted and unweighted models showed remarkable difference in terms of the network grouping and correlation between nodes (Fig. 8A). Most notably, the edges surrounding TM5, TM6, and TM7, and the binding site displayed higher correlations compared to the remaining edges in the WAY-267,464-bound system. The number of high correlated connections depicted by thicker edges, were found to be higher in WAY-267,464-bound system than in WAY-Methylated-bound system (Fig. 8B). Groups of residues with frequent and strong interactions were found to be completely different in terms of their arrangement and size (Fig. 8/C, D). There is a total of 12 respective communities connected by critical edges (Figs. 1/E, F).

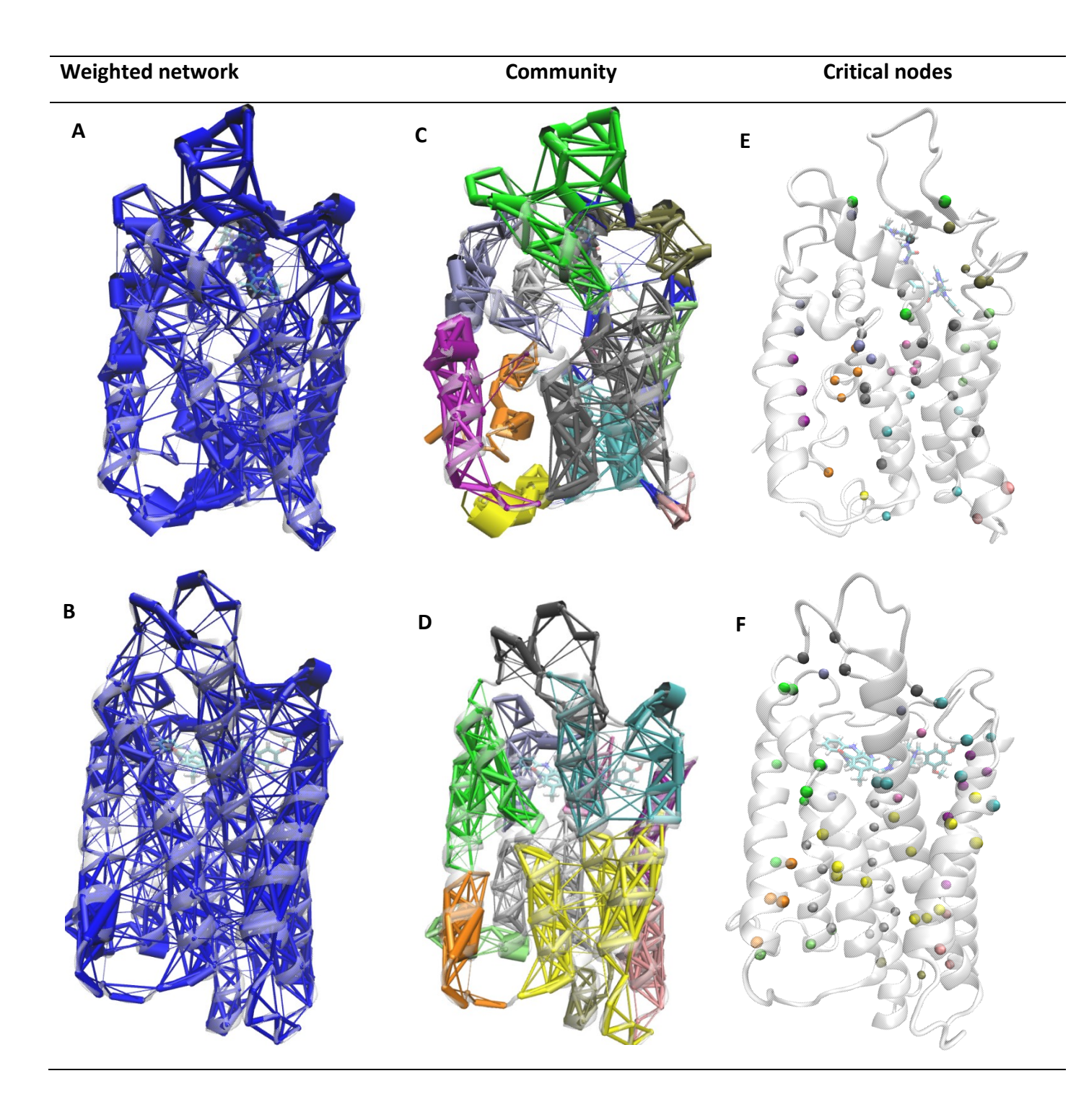


Fig. 8. Weighted networks, communities and critical nodes of WAY-267,464- (A) and WAY-methylated-bound OTR (B). The weight of the network is indicated by the thickness of the edge. There are 12 communities connected by critical nodes.

3.7. Optimal paths revealed key residues involved in the shortest pathway for passing a signal from WAY-267,464 and WAY-Methylated to the molecular switches.

From the weighted network models, we identified the shortest pathways for signal transmission from ligand binding site to the molecular switches (transmission switch at Trp297, and ionic lock switch at Asp136, and tyrosine toggle switch at Tyr329). Although a common potential signal source (Lys116^{3.29}) was used, each optimal path generated was unique. The path of communication between WAY-267,464 and ionic lock (DRY), D136^{3,49} was completely along TM3 and comprised Lys116, Leu118, Vall21, Gly122, Ser126, Leu130, Met133, Asp136^{3.49} (Fig. 9A), whereas the corresponding path in the WAY-Methylated bound system comprised Lys116, Gln119, Met123, Tyr128, Leu132, Met133 and Asp136^{3.49} (Fig. 9B). For the tyrosine toggle switch (NPXXY), the WAY-267,464's optimal path sent signals primarily along TM3, TM2 and TM7, and the residues involved were Lys116, Leu118, Val121, Ala84, Ser82, Asn325, and Tyr329^{7.53} (Fig. 9C), whereas the corresponding path in WAY-Methylated system comprised Lys116, Leu118, Met123, Ser126, Leu81, and Tyr329^{7.53} (**Fig. 9D**). In case of transmission switch (CWXP), longer optimal path was found in the WAY-267,464-bound system along TM3, TM1, TM2, TM7 and TM6 and comprises residues K116, F91, D92, L50, L48, A45, A318, L317, Q295, and W297^{6.57}(Fig. 9E). The corresponding shorter optimal path in the WAY-Methylated-bound system was along K116, Q119, M123, F292, F293, W297^{6.57} (Fig. 9F). This path, which was along only TM3 and TM6, was found to be the shortest among all the 3 optimal paths generated in both agonist WAY-267,464- and antagonist WAY-Methylated bound systems. The corresponding suboptimal paths of each system are given in the supplementary information file (Fig. S12).

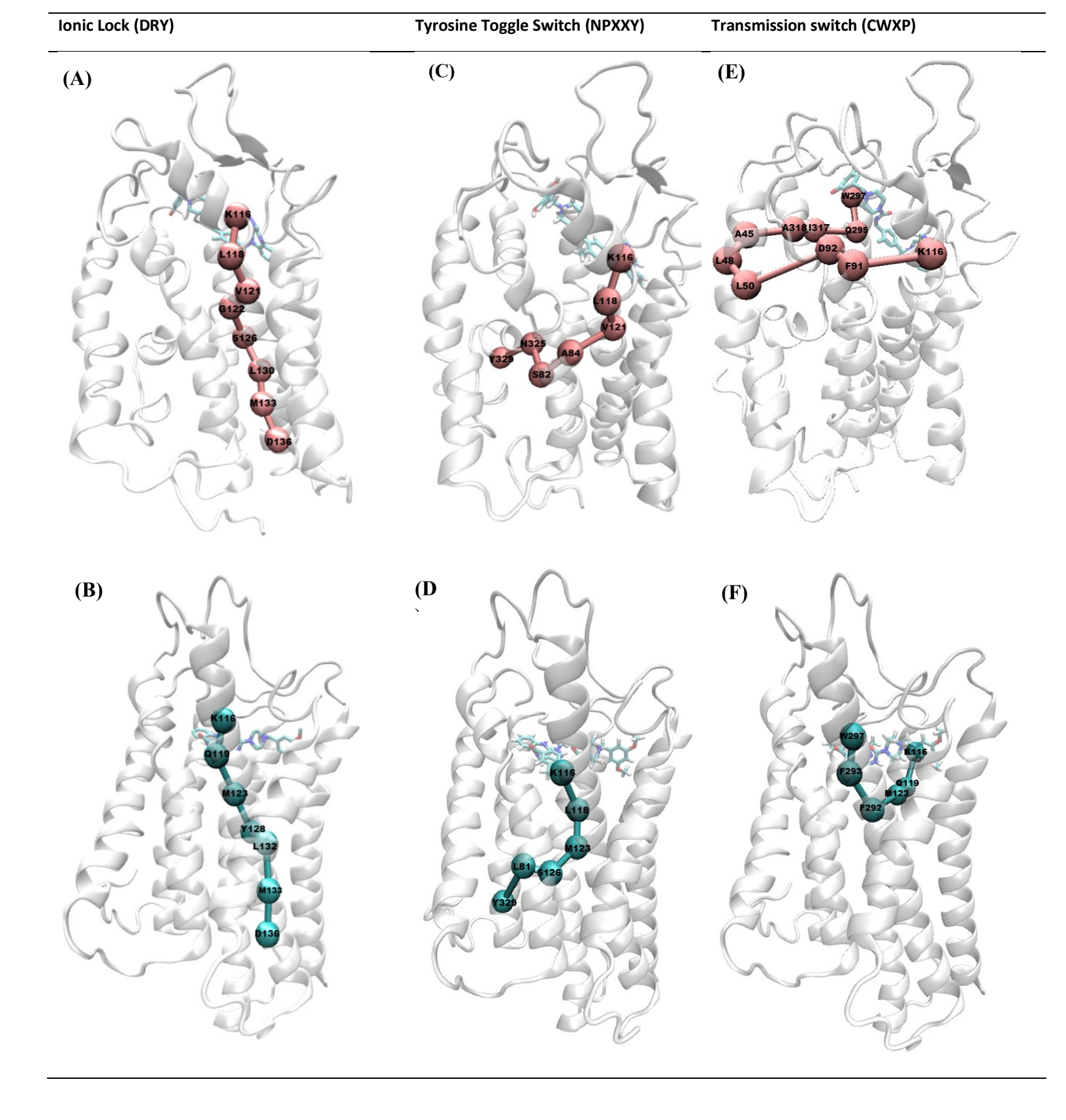


Fig. 9. Optimal path of communication from WAY-267,464 (A) and WAY-Methylated binding sites (B) to the ionic lock (DRY) (D136^{3.49}); to the tyrosine toggle switch (NPXXY) (Y329^{7.53})

from WAY-267,464 (C) and WAY-Methylated (D); and to the transmission switch (CWXP), (W297^{6.57}) from WAY-267,464 (E), and WAY-Methylated (F).

3.8. Cross referencing the critical nodes with mutagenesis data allows for identification of residues that may play an important role in the OTR activation

A total of 43 critical nodes were identified in the WAY-267,464 system out of which 7 residues, Asn57, Met78, Asp85, Pro197, Tyr209, Phe284, and MET315 were found to correspond to experimentally reported mutagenesis data available on the G-protein coupled receptor databank (GPCRdb) (Fig. 10/A, B). For WAY-Methylated system, a total of 47 critical residues were identified out of which only 3 residues, Met123, Asp136, Phe284 overlap with the mutagenesis data. However, these residues in both WAY-267,464- (Fig. 10C) and WAY-methylated-bound systems (Fig. 10D) fall in the category of in vitro mutant with No/low effect (<5-fold). Interestingly, only one residue, Phe284, was found to be present in both systems. The remaining 6 critical residues, Asn57, Met78, Asp85, Pro197, Tyr209, Phe284, And Met315, uniquely identified in the WAY-267,464-bound system, may be critical for the activation of the receptor.

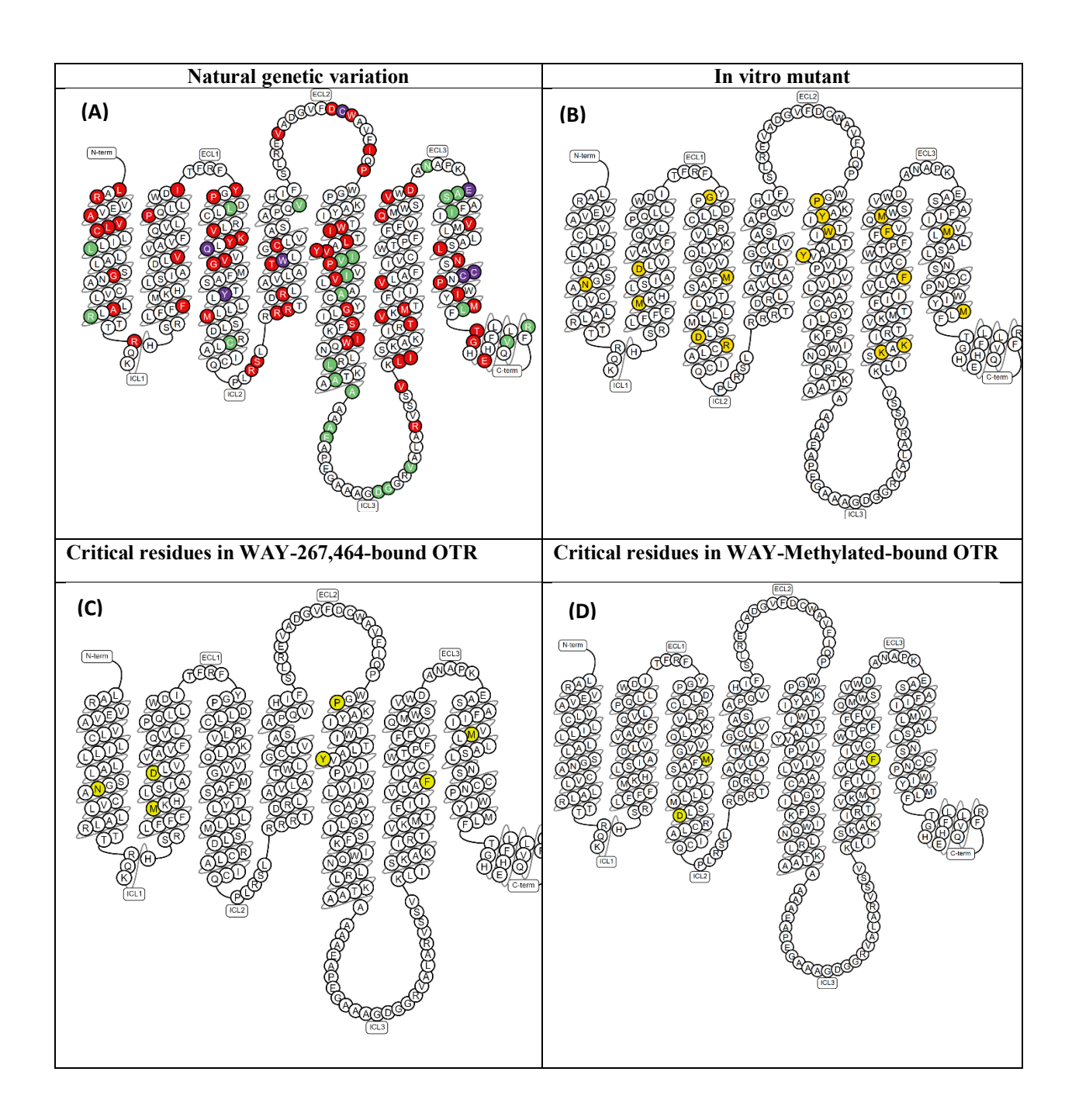


Fig. 10. Reported mutagenesis data for the OTR. Mutated residues in red cause decrease in activity, green cause increase in activity and purple is a deleterious stop gained mutation (A). In vitro Mutant Data: Increased binding/potency: >5-fold, >10-fold; Reduced binding/potency: >5-fold, >10-fold; No/low effect (<5-fold) (B). The critical nodes in WAY-267,464-bound OTR (C) and WAY-Methylated-bound OTR that overlap with the mutation data.

Discussion

OTR is a well validated target: The OTR has been a therapeutic target for inducing/delaying labor, treating erectile dysfunction, and for a variety of anxiety and social disorders. Due to the highly conserved nature of the OTR and the vasopressin receptors, it is very difficult to create a ligand selective for OTR only. Currently, the only FDA approved ligands targeting the OTR are peptides, which display many unfavorable pharmacological properties and side effects, prompting the search for non-peptide ligands — an endeavor hindered by both a lack of detailed molecular interactions information and the absence of a high-resolution crystal structure of OTR. Previous computational studies on the OTR ran very short MD simulations; under than 5 ns long [8, 9, 18, 72, 73], and only used the standard unrestrained (AutoDock) docking methods to determine a single binding pose and then relied on the docking score to determine ligand binding strength [4, 8, 9, 72-74]. Unlike these methods, Glide approximates a complete systematic search for conformational, orientational and positional space of the docked ligand to dramatically narrows the search space, followed by torsionally flexible energy optimization on an OPLS-AA nonbonded potential grid for few hundred surviving candidates poses. The best candidates are further refined via a Monte Carlo sampling of pose conformation [43].

Different docking methods yields alternative ligand binding poses: We generated multiple docking poses using standard docking procedures in combination with positional constraints to invert the ligands within the receptor binding pocket, utilized 2 μs MD simulations to further optimize the binding poses, and then used the docking scores as well as MM-GBSA binding energy calculations to choose the most favorable binding pose for each ligand. These binding poses were validated by experimental evidence including mutagenesis studies listing key residues involved in ligand binding. Docking scores are an empirical binding score calculation

which keep the receptor in a rigid state, while MM-GBSA are based on physics methods which consider the conformational energy change induced upon complex formation. By considering the conformational energy change and by allowing the receptor to be more flexible during the simulation, MM-GBSA binding energy scores result in a better binding affinity prediction than docking scores. Having multiple binding poses in addition to running extended MD simulations may enhance the sampling of ligand binding poses, thus improving the overall accuracy of the computational prediction. Given the recent increases in computing power, this type of novel methodology may be applied to other GPCRs.

Transition from inactive state to active state is observed in WAY-267,464-bound system: The homology model of OTR built in the present study is based on the inactive conformation of the nociception receptor; therefore, its default configuration is an inactive state. The transition from inactive state to active state requires the binding of an agonist, which results in more structural deviation/residual fluctuation to aid in this conformational shift. This trend was observed in our data; the ligand RMSF mean value was over twice larger for agonist WAY-267,464-bound system (2.67 Å) than for the antagonist WAY-Methylated-bound system (1.05 Å). Overall, the protein RMSF values for the agonist-bound OTR were larger than that of the antagonist-bound OTR by 0.54 Å. The structural data from both complexes showed that the most significant changes occurred around TM6, intracellular loop 3, and extracellular loop 3. Comparing between the two complexes, the mean RMSF values of WAY-267,464 were larger than those for WAY-Methylated by 1.19 Å, 5.65 Å, and 1.28 Å for TM6, I3, and E3, respectively. These structural aberrations can be better understood based on our secondary structure data, which showed that, the WAY-Methylated complex induced more helix formation in the receptor by 14.95%, mainly in TMs 6 and 7. This increase in secondary structure may have aided in stabilizing the receptor

and decreasing fluctuations. The methylation of the resorcinol moiety in WAY-267,464 increased the hydrophobicity of the ligand, which may help explain why WAY-Methylated bound deeper into the binding pocket than WAY-267,464 did. The OTR's response was stabilizing the initial inactive conformation by decreasing fluctuations and increasing the total secondary structure composition. On the other hand, the agonist WAY-267,464 induced fluctuations, specifically in TM6, I3, and E3, from the default inactive state to an active state to enable the receptor to interact with downstream proteins to result in cellular responses. A previous study by our group showed that agonists for the opium receptor induce larger fluctuations compared with antagonist [75].

OTR can be considered a 'nonselective' vasopressin receptor [76]. The OTR has equal affinity for vasopressin and oxytocin, whereas the V₁R has a 30-fold higher affinity for vasopressin than for oxytocin [77]. WAY-267,464 was initially reported to have 100-fold greater selectivity for the OTR relative to the V_{1A}R [30]. WAY-267,464 was later shown to function as a V_{1A}R antagonist while having only relatively weak OTR agonist actions in vitro [78]. Here, even though there are no MD simulation data on V_{1A}R available to allow for meaningful comparison of ligand-induced conformational changes, consistent with the in vitro study, our findings suggest that the WAY-267,464-bound OTR may be in a state of partial activation.

Dynamics network analysis identify possible signal transduction pathways: Molecular switches enable signal flow from the agonist binding site, usually located close to the extracellular surface, to the intracellular part of the receptor. The switches are usually associated with conserved TM motifs [79]. We examined 3 canonical molecular switches in both simulated complexes. The tyrosine toggle switch is on in the antagonist WAY-Methylated system,

suggesting inactivation; and off in the agonist WAY-267,848 system, suggesting activation. This difference was due the complete flipping of Tyr329 in the WAY-267,464 system, but this change was not seen in the WAY-Methylated system. However, even though movement of TM6 towards TM5 was observed at the transmission switch, the torsion angle profile of Trp297 did not show a large difference between the two systems. Similarly, contrary to the known format of class A GPCR activation [71], the ASP136-Lys270 ionic lock switch was found to be broken in both systems. Furthermore, as successfully applied recently [80], we employed dynamic network model to identify critical residues and determine potential signal transduction pathways from the ligand binding site to each of these molecular switches. The critical residues were then crossreferenced with the experimentally determined mutagenesis data. We found a total of 6 residues unique to agonist WAY-267,864-bound system that overlap with in vitro mutation data: Asn57 [81], Met78 and Met315 [82], Asp85 and Try209 [83] and Pro197 [84]. For WAY-Methylated system, 2 critical residues overlap with *in vitro* mutation data: Met123 [82] and Asp136 [18], whereas only Phe284 [83] was found to be in common to both systems. This higher number of critical residues identified in the agonist WAY-267,464 system may help explain the transition between the two states of the receptor, thereby further supporting our conformational dynamics model.

Conclusions

Non-peptide ligands of OTR have promising potential as therapeutic agents with improved pharmacological properties. Interestingly, non-peptide OTR agonist WAY-267,464 becomes a partial antagonist when the resorcinol moiety is methylated. Here, we utilized positional constraints to probe alternative binding poses of these non-peptide ligands and computed their

MM-GBSA binding energy following an extended 2μS MD simulation. The added methyl groups enhanced hydrophobicity, resulting in a flipped binding pose deeper in the binding pocket. Stabilization of the initial inactive conformation, decreasing fluctuations by increasing the overall secondary structural composition were the response to the methylation. WAY-267,464 induced larger fluctuations to allow the receptor to change from the default inactive state to an active conformation. Molecular switch examination and network analysis identified critical residues which overlap with *in vitro* mutagenesis data. These findings may further support our conformational dynamics models explaining the opposing activities of these structurally related ligands.

Supporting Information

The sequence with genetic numbering of the human OTR and the built model of OTR; the atoms used in the positional constraint for DGV; WAY-267,464, and WAY-Methylated; the RMSD plots for XP and PC docked WAY-267,464 and WAY-Methylated in the short initial MD simulations; the complex structures chosen for the longer MD simulations; the representative complex structures for each cluster of the extended simulations; the protein residue-ligand interaction plots and contact histograms for the short initial MD simulations; Molecular switches profiles; and suboptimal paths of communication between WAY-267,464 and WAY-Methylated binding sites and molecular switches are also provided.

Acknowledgements

We acknowledge the High Performance Computing Facility at Rowan funded by the National Science Foundation under Grants MRI- 1429467 and XSEDE MCB160004/160164/160173. The grants from National Natural Science Foundation of China (11575021, U1530402) to H.L. are acknowledged.

References

- 1. Viero, C., et al., *Oxytocin: Crossing the Bridge between Basic Science and Pharmacotherapy.* Cns Neuroscience & Therapeutics, 2010. **16**(5): p. e138-e156.
- 2. Weill, N., et al., *Identification of Nonpeptide Oxytocin Receptor Ligands by Receptor-Ligand Fingerprint Similarity Search.* Molecular Informatics, 2011. **30**(6-7): p. 521-526.
- 3. Koehbach, J., et al., *Insights into the molecular evolution of oxytocin receptor ligand binding.* Biochemical Society Transactions, 2013. **41**: p. 197-+.
- 4. Slusarz, M.J., E. Sikorska, and R. Slusarz, *Interactions of vasopressin and oxytocin receptors with vasopressin analogues substituted in position 2 with 3,3 '-diphenylalanine a molecular docking study.* Journal of Peptide Science, 2013. **19**(2): p. 118-126.
- 5. Busnelli, M., et al., Selective and Potent Agonists and Antagonists for Investigating the Role of Mouse Oxytocin Receptors. Journal of Pharmacology and Experimental Therapeutics, 2013. **346**(2): p. 318-327.
- 6. Wootten, D.L., et al., *Agonist-specific requirement for a glutamate in transmembrane helix 1 of the oxytocin receptor.* Molecular and Cellular Endocrinology, 2011. **333**(1): p. 20-27.
- 7. Wheatley, M., et al., Extracellular loops and ligand binding to a subfamily of Family A G-protein-coupled receptors. Biochemical Society Transactions, 2007. **35**: p. 717-720.
- 8. Slusarz, M.J., R. Susarz, and J. Ciarkowski, *Molecular dynamics simulation of human* neurohypophyseal hormone receptors complexed with oxytocin modeling of an activated state. Journal of Peptide Science, 2006. **12**(3): p. 171-179.
- 9. Slusarz, M.J., et al., Study of new oxytocin antagonist barusiban (Fe200 440) affinity toward human oxytocin receptor versus vasopressin V1a and V2 receptors Molecular dynamics simulation in POPC bilayer. Qsar & Combinatorial Science, 2005. **24**(5): p. 603-610.
- 10. Mouillac, B., et al., *The binding site of neuropeptide vasopressin V1a receptor. Evidence for a major localization within transmembrane regions.* J Biol Chem, 1995. **270**(43): p. 25771-7.
- 11. Kwiatkowska, A., et al., *Novel analogues of arginine vasopressin containing alpha-2-indanylglycine enantiomers in position 2.* Journal of Peptide Science, 2010. **16**(1): p. 15-20.
- 12. Kwiatkowska, A., et al., *Design, synthesis and biological activity of new neurohypophyseal hormones analogues conformationally restricted in the N-terminal part of the molecule. Highly potent OT receptor antagonists.* Amino Acids, 2012. **43**(2): p. 617-627.
- 13. Jorgensen, W.T., et al., *Flexible analogues of WAY-267,464: Synthesis and pharmacology at the human oxytocin and vasopressin 1(a) receptors.* European Journal of Medicinal Chemistry, 2016. **108**: p. 730-740.
- 14. Griffante, C., et al., Selectivity of d Cha(4) AVP and SSR149415 at human vasopressin and oxytocin receptors: evidence that SSR149415 is a mixed vasopressin V-1b/oxytocin receptor antagonist. British Journal of Pharmacology, 2005. **146**(5): p. 744-751.
- 15. Gravati, M., et al., *Dual modulation of inward rectifier potassium currents in olfactory neuronal cells by promiscuous G protein coupling of the oxytocin receptor.* Journal of Neurochemistry, 2010. **114**(5): p. 1424-1435.
- 16. Gonzalez-Iglesias, A.E., et al., *Direct Stimulatory Effects of Oxytocin in Female Rat Gonadotrophs and Somatotrophs In Vitro: Comparison With Lactotrophs.* Endocrinology, 2015. **156**(2): p. 600-612.
- 17. Gimpl, G., et al., Oxytocin receptors: ligand binding, signalling and cholesterol dependence, in Advances in Vasopressin and Oxytocin: From Genes to Behaviour to Disease, I.D. Neumann and R. Landgraf, Editors. 2008, Elsevier Science Bv: Amsterdam. p. 193-204.
- 18. Favre, N., et al., *The DRY motif as a molecular switch of the human oxytocin receptor.* Biochemistry, 2005. **44**(30): p. 9990-10008.

- 19. Chini, B. and M. Manning, *Agonist selectivity in the oxytocin/vasopressin receptor family: new insights and challenges.* Biochemical Society Transactions, 2007. **35**: p. 737-741.
- 20. Ashworth, D.M., et al., *Nonpeptide Oxytocin Agonists*. Drugs of the Future, 2006. **31**(4): p. 345-353.
- 21. Sharma, A., et al., Functional involvement of protein kinase C, Rho-kinase and TRPC3 decreases while PLC increases with advancement of pregnancy in mediating oxytocin-induced myometrial contractions in water buffaloes (Bubalus bubalis). Theriogenology, 2017. **92**: p. 176-189.
- 22. Gram, A., A. Boos, and M.P. Kowalewski, *Uterine and Placental Expression of Canine Oxytocin Receptor During Pregnancy and Normal and Induced Parturition.* Reproduction in Domestic Animals, 2014. **49**: p. 41-49.
- 23. Chatterjee, O., et al., *An overview of the oxytocin-oxytocin receptor signaling network.* Journal of Cell Communication and Signaling, 2016. **10**(4): p. 355-360.
- 24. Cattaneo, M.G., G. Lucci, and L.M. Vicentini, *Oxytocin stimulates in vitro angiogenesis via a Pyk-2/Src-dependent mechanism*. Experimental Cell Research, 2009. **315**(18): p. 3210-3219.
- 25. Hicks, C., et al., WAY 267,464, a non-peptide oxytocin receptor agonist, impairs social recognition memory in rats through a vasopressin 1A receptor antagonist action. Psychopharmacology, 2015. **232**(15): p. 2659-2667.
- 26. Hicks, C., et al., Body temperature and cardiac changes induced by peripherally administered oxytocin, vasopressin and the non-peptide oxytocin receptor agonist WAY 267,464: a biotelemetry study in rats. British Journal of Pharmacology, 2014. **171**(11): p. 2868-2887.
- 27. Hicks, C., et al., *The nonpeptide oxytocin receptor agonist WAY 267,464: receptor-binding profile, prosocial effects and distribution of c-Fos expression in adolescent rats.* J Neuroendocrinol, 2012. **24**(7): p. 1012-29.
- 28. Manning, M., et al., *Oxytocin and Vasopressin Agonists and Antagonists as Research Tools and Potential Therapeutics.* Journal of Neuroendocrinology, 2012. **24**(4): p. 609-628.
- 29. Reekie, T.A., I.S. McGregor, and M. Kassiou, *Pyrazolo 1,4 diazepines as non-peptidic probes of the oxytocin and vasopressin receptorOTs.* Tetrahedron Letters, 2014. **55**(33): p. 4568-4571.
- 30. Ring, R.H., et al., *Receptor and behavioral pharmacology of WAY-267464, a non-peptide oxytocin receptor agonist*. Neuropharmacology, 2010. **58**(1): p. 69-77.
- 31. Olszewski, P.K., et al., *A non-peptide oxytocin receptor agonist, WAY-267,464, alleviates novelty-induced hypophagia in mice: Insights into changes in c-Fos immunoreactivity.* Pharmacology Biochemistry and Behavior, 2014. **124**: p. 367-372.
- Wheatley, M., et al., *Agonist binding to peptide hormone receptors*. Biochemical Society Transactions, 2003. **31**: p. 35-39.
- 33. Busnelli, M., et al., *Design and Characterization of Superpotent Bivalent Ligands Targeting Oxytocin Receptor Dimers via a Channel-Like Structure*. Journal of Medicinal Chemistry, 2016. **59**(15): p. 7152-7166.
- 34. Koehbach, J., et al., *Insights into the molecular evolution of oxytocin receptor ligand binding.* Biochemical Society Transactions, 2013. **41**(1): p. 197-+.
- 35. Harder, E., et al., *OPLS3: A Force Field Providing Broad Coverage of Drug-like Small Molecules and Proteins.* Journal of Chemical Theory and Computation, 2016. **12**(1): p. 281-296.
- 36. Magrane, M. and U. Consortium, *UniProt Knowledgebase: a hub of integrated protein data.* Database (Oxford), 2011. **2011**: p. bar009.
- 37. Jacobson, M.P., et al., *A hierarchical approach to all-atom protein loop prediction.* Proteins-Structure Function and Bioinformatics, 2004. **55**(2): p. 351-367.
- 38. Jacobson, M.P., et al., *On the Role of the Crystal Environment in Determining Protein Side-chain Conformations*. Journal of Molecular Biology, 2002. **320**(3): p. 597-608.

- 39. Miller, R.L., et al., *The importance of ligand-receptor conformational pairs in stabilization: spotlight on the N/OFQ G protein-coupled receptor.* Structure (London, England : 1993), 2015. **23**(12): p. 2291-2299.
- 40. Lomize, M.A., et al., *OPM database and PPM web server: resources for positioning of proteins in membranes.* Nucleic Acids Research, 2012. **40**(D1): p. D370-D376.
- 41. Sastry, G.M., et al., *Protein and ligand preparation: parameters, protocols, and influence on virtual screening enrichments.* J Comput Aided Mol Des, 2013. **27**(3): p. 221-34.
- 42. Friesner, R.A., et al., Extra precision glide: Docking and scoring incorporating a model of hydrophobic enclosure for protein-ligand complexes. Journal of Medicinal Chemistry, 2006. **49**(21): p. 6177-6196.
- 43. Friesner, R.A., et al., *Glide: A new approach for rapid, accurate docking and scoring. 1. Method and assessment of docking accuracy.* Journal of Medicinal Chemistry, 2004. **47**(7): p. 1739-1749.
- 44. Lyman, E., et al., A Role for a Specific Cholesterol Interaction in Stabilizing the Apo Configuration of the Human A(2A) Adenosine Receptor. Structure, 2009. **17**(12): p. 1660-1668.
- 45. Mark, P. and L. Nilsson, *Structure and dynamics of the TIP3P, SPC, and SPC/E water models at 298 K.* Journal of Physical Chemistry A, 2001. **105**(43): p. 9954-9960.
- 46. Zhang, J., et al., *The LBFGS quasi-Newtonian method for molecular modeling prion AGAAAAGA amyloid fibrils.* Natural Science, 2012. **04**(12): p. 1097-1108.
- 47. Ikeguchi, M., *Partial rigid-body dynamics in NPT, NPAT and NP gamma T ensembles for proteins and membranes.* Journal of Computational Chemistry, 2004. **25**(4): p. 529-541.
- 48. Bailey, A.G. and C.P. Lowe, *MILCH SHAKE: An Efficient Method for Constraint Dynamics Applied to Alkanes.* Journal of Computational Chemistry, 2009. **30**(15): p. 2485-2493.
- 49. Shan, Y.B., et al., *Gaussian split Ewald: A fast Ewald mesh method for molecular simulation.*Journal of Chemical Physics, 2005. **122**(5): p. 54101.
- 50. Stuart, S.J., R.H. Zhou, and B.J. Berne, *Molecular dynamics with multiple time scales: The selection of efficient reference system propagators.* Journal of Chemical Physics, 1996. **105**(4): p. 1426-1436.
- 51. Kevin J. Bowers, E.C., Huafeng Xu, Ron O. Dror, Michael P. Eastwood,, J.L.K. Brent A. Gregersen, Istvan Kolossvary, Mark A. Moraes, Federico D. Sacerdoti,, and Y.S. John K. Salmon, David E. Shaw, *Scalable Algorithms for Molecular Dynamics*

Simulations on Commodity Clusters. 2006.

- 52. Ghosh, A., C.S. Rapp, and R.A. Friesner, *Generalized born model based on a surface integral formulation*. Journal of Physical Chemistry B, 1998. **102**(52): p. 10983-10990.
- 53. Yu, Z.Y., M.P. Jacobson, and R.A. Friesner, *What role do surfaces play in GB models? A new-generation of surface-generalized Born model based on a novel Gaussian surface for biomolecules.* Journal of Computational Chemistry, 2006. **27**(1): p. 72-89.
- 54. Li, J., et al., *The VSGB 2.0 model: A next generation energy model for high resolution protein structure modeling.* Proteins-Structure Function and Bioinformatics, 2011. **79**(10): p. 2794-2812.
- 55. Harder, E., et al., *OPLS3: A Force Field Providing Broad Coverage of Drug-like Small Molecules and Proteins.* J Chem Theory Comput, 2016. **12**(1): p. 281-96.
- 56. Jorgensen, W.L., D.S. Maxwell, and J. TiradoRives, *Development and testing of the OPLS all-atom force field on conformational energetics and properties of organic liquids*. Journal of the American Chemical Society, 1996. **118**(45): p. 11225-11236.
- 57. Kongsted, J., P. Soderhjelm, and U. Ryde, *How Accurate are Continuum Solvation Models for Drug-Like Molecules?* J. Comput.-Aided Mol. Des., 2009. **23**(7): p. 395-409.
- 58. Kollman, P., et al., *Calculating Structures and Free Energies of Complex Molecules: Combining Molecular Mechanics and Continuum Models.* Acc. Chem. Res., 2000. **33**(12): p. 889-897.

- 59. Hou, T., et al., Assessing the Performance of the Molecular Mechanics/Poisson Boltzmann Surface Area and Molecular Mechanics/Generalized Born Surface Area Methods. II. The Accuracy of Ranking Poses Generated from Docking. J. Comput. Chem., 2010. **32**(5): p. 866-877.
- 60. Hou, T., et al., Assessing the Performance of the MM/PBSA and MM/GBSA Methods. 1. The Accuracy of Binding Free Energy Calculations Based on Molecular Dynamics Simulations. J. Chem. Inf. Model., 2011. **51**(1): p. 69-82.
- 61. Xu, L., et al., Assessing the Performance of MM/PBSA and MM/GBSA Methods. 3. The Impact of Force Fields and Ligand Charge Models. J. Phys. Chem. B., 2013. **117**(28): p. 8408-8421.
- 62. Sun, H., et al., Assessing the Performance of MM/PBSA and MM/GBSA Methods. 4. Accuracies of MM/PBSA and MM/GBSA Methodologies Evaluated by Various Simulation Protocols Using PDBbind Data Set. PCCP, 2014. **16**(31): p. 16719-16729.
- 63. Eargle, J. and Z. Luthey-Schulten, *NetworkView: 3D display and analysis of protein-RNA interaction networks*. Bioinformatics (Oxford, England), 2012. **28**(22): p. 3000-3001.
- 64. Humphrey, W., Dalke, A. and Schulten, K, "VMD Visual Molecular Dynamics". J. Molec. Graphics, 1996. **14**: p. 33-38.
- 65. Glykos, N.M., *Software news and updates. Carma: a molecular dynamics analysis program.* J Comput Chem, 2006. **27**(14): p. 1765-8.
- 66. Girvan, M. and M.E.J. Newman, *Community structure in social and biological networks.*Proceedings of the National Academy of Sciences, 2002. **99**(12): p. 7821.
- 67. Liu, H.B., et al., *Molecular mechanism of action for reversible P2Y(12) antagonists.* Biophysical Chemistry, 2011. **155**(2-3): p. 74-81.
- 68. Yang, M., et al., Lysine 270 in the third intracellular domain of the oxytocin receptor is an important determinant for G alpha(q) coupling specificity. Molecular Endocrinology, 2002. **16**(4): p. 814-823.
- 69. Strunecka, A., S. Hynie, and V. Klenerova, *Role of Oxytocin/Oxytocin Receptor System in Regulation of Cell Growth and Neoplastic Processes*. Folia Biologica, 2009. **55**(5): p. 159-165.
- 70. Kobilka, B.K. and X. Deupi, *Conformational complexity of G-protein-coupled receptors*. Trends in Pharmacological Sciences, 2007. **28**(8): p. 397-406.
- 71. Trzaskowski, B., et al., *Action of Molecular Switches in GPCRs Theoretical and Experimental Studies*. Current Medicinal Chemistry, 2012. **19**(8): p. 1090-1109.
- 72. Jojart, B. and A. Marki, *Possible dynamic anchor points in a benzoxazinone derivative-human oxytocin receptor system a molecular docking and dynamics calculation.* Journal of Molecular Modeling, 2007. **13**(1): p. 1-10.
- 73. Slusarz, M.J., R. Slusarz, and J. Ciarkowski, *Investigation of mechanism of desmopressin binding in vasopressin V2 receptor versus vasopressin V1a and oxytocin receptors: Molecular dynamics simulation of the agonist-bound state in the membrane-aqueous system.* Biopolymers, 2006. **81**(5): p. 321-338.
- 74. Slusarz, M.J., et al., Molecular docking-based study of vasopressin analogues modified at positions 2 and 3 with N-methylphenylalanine: Influence on receptor-bound conformations and interactions with vasopressin and oxytocin receptors. Journal of Medicinal Chemistry, 2006. **49**(8): p. 2463-2469.
- 75. Sader, S., K. Anant, and C. Wu, To probe interaction of morphine and IBNtxA with 7TM and 6TM variants of the human μ -opioid receptor using all-atom molecular dynamics simulations with an explicit membrane. Physical Chemistry Chemical Physics, 2018. **20**(3): p. 1724-1741.
- 76. Holmes, C.L., D.W. Landry, and J.T. Granton, Critical Care, 2003. **7**(6).
- 77. Peter, J., et al., *Molecular neurobiology and pharmacology of the Vasopressin/Oxytocin receptor family.* Cellular and Molecular Neurobiology, 1995. **15**(5): p. 573-595.

- 78. Hicks, C., et al., *The Nonpeptide Oxytocin Receptor Agonist WAY 267,464: Receptor-Binding Profile, Prosocial Effects and Distribution of c-Fos Expression in Adolescent Rats.* Journal of Neuroendocrinology, 2012. **24**(7): p. 1012-1029.
- 79. Filipek, S., *Molecular switches in GPCRs.* Current Opinion in Structural Biology, 2019. **55**: p. 114-120.
- 80. Li, Q., et al., *Dynamical important residue network (DIRN): network inference via conformational change.* Bioinformatics, 2019. **35**(22): p. 4664-4670.
- 81. Fanelli, F., et al., Activation mechanism of human oxytocin receptor: a combined study of experimental and computer-simulated mutagenesis. Mol Pharmacol, 1999. **56**(1): p. 214-25.
- 82. Breton, C., et al., *Direct identification of human oxytocin receptor-binding domains using a photoactivatable cyclic peptide antagonist: comparison with the human V1a vasopressin receptor.* J Biol Chem, 2001. **276**(29): p. 26931-41.
- 83. Gimpl, G. and F. Fahrenholz, *The oxytocin receptor system: structure, function, and regulation.* Physiol Rev, 2001. **81**(2): p. 629-83.
- 84. Politowska, E., et al., *Molecular modelling study of the role of cholesterol in the stimulation of the oxytocin receptor*. Acta Biochimica Polonica, 2001. **48**(1): p. 83-93.